Electrons in GaAs/$Ga_{1-x}Al_xAs$ superlattices: Spin and orbital states in a magnetic field

Pawel Pfeffer* and Wlodek Zawadzki
Institute of Physics, Polish Academy of Sciences, Al. Lotnikow 32/46, 02-668 Warsaw, Poland
(Received 19 November 2009; revised manuscript received 23 January 2010; published 9 June 2010)

Spin and orbital properties of electrons in GaAs/$Ga_{1-x}Al_xAs$ superlattices (SLs) in an external longitudinal and transverse magnetic field are considered. A five-level $\mathbf{P}\cdot\mathbf{p}$ model of the band structure is used, accounting for nonparabolicity and nonsphericity of the conduction band in III-V compounds as well as their inversion asymmetry. The electron-spin g values are computed as functions of superlattice spacings. It is shown that, in the transverse-field configuration, the g value is different for various electron locations in an SL. Transverse and longitudinal cyclotron masses are calculated and compared with available experimental data for various GaAs/$Ga_{1-x}Al_xAs$ SLs. Finally, orbital electron states in short SLs in a transverse magnetic field are described for different field intensities. In addition to the standard Landau levels unexpected states are found whose energies have a strong quadraticlike field dependence. The origin of the states is investigated.

DOI: 10.1103/PhysRevB.81.235310 PACS number(s): 73.20.At, 73.21.Cd, 73.21.Fg

I. INTRODUCTION

Electrons in semiconductor superlattices (SLs) have been a subject of intensive studies because of their inherent fundamental properties as well as important applications. Superlattices, since their creation in the early 1970,[1] belong with other heterostructures to "hand-made" quantum systems. From their beginning SLs were treated theoretically by methods developed earlier for atomic crystals. Thus, the standard notions of Bloch functions, energy bands, forbidden gaps, and Brillouin zones were employed for their description.[2–5] As far as experimental studies are concerned, an external magnetic field was extensively used as an important tool both in optical and transport investigations. Physically, different situations are created for a magnetic field $\mathbf{B}$ parallel or transverse to the growth direction. For $\mathbf{B}_\parallel$ (parallel to the growth direction), one can separate the motion into an electric component along the growth and a magnetic component transverse to the growth (parallel to interfaces). On the other hand, for $\mathbf{B}_\perp$ (transverse to the growth), the motion cannot be separated since both the periodic potential of an SL and the magnetic field $\mathbf{B}_\perp$ affect the motion along the growth.

The orbital and the spin properties of electrons are usually characterized by an effective mass m^* and an effective spin (Lande) factor g^*, respectively. As to electrons in SLs, one studied mostly the effective masses while little attention was paid to the spin g values. Wu *et al.*[4] calculated spin energies in $Ga_{0.47}In_{0.53}As/Al_{0.48}In_{0.52}As$ superlattices without discussing the g values. The recent interest in spintronics makes the electron-spin properties in various systems of primary importance. Thus, we investigate the behavior of the electron spin in SLs. In addition, we study theoretically also some orbital-electron properties in short SLs and, in particular, we report on unexpected electron energies and states in the transverse-field configuration $\mathbf{B}_\perp$.

We consider III-V SLs and, more specifically, the GaAs/$Ga_{1-x}Al_xAs$ system. Among numerous heterostructures, the system GaAs/$Ga_{1-x}Al_xAs$ has a unique position. First, GaAs is after silicon the most important semiconductor material. Second, the system GaAs/$Ga_{1-x}Al_xAs$ has well-established parameters which allows the theorists to describe subtle phenomena. Third, due to the advanced growth technology the electrons in GaAs quantum wells have very high mobilities making it possible to detect even weak effects. Thus, it is of interest to describe precisely spin and orbital electron energies in GaAs/$Ga_{1-x}Al_xAs$ quantum wells not only for their own sake but also as a model for other heterostructures. From the theoretical point of view, a description of magneto-optical effects in GaAs-type materials is not an easy task since GaAs is a medium-gap semiconductor. As a result, its band structure exhibits features characteristic of the narrow-gap materials, but it is insufficient to treat them by the models normally used for such systems. We showed in our previous work on bulk GaAs and InP that the simplest adequate description of their band structure is given by the so-called five-level $\mathbf{P}\cdot\mathbf{p}$ model (5LM, see Ref. 6). The usefullness of 5LM was confirmed in the work with quantum wells,[7,8] so we use this model in our present calculations.

An important feature of the III-V compounds is a bulk-inversion asymmetry (BIA) of these materials. As is known for a long time,[9] the BIA results in a spin splitting of energies for a given direction of the wave vector $\mathbf{k}$. It is of interest to investigate how this spin splitting behaves in the presence of an external magnetic field. One can rephrase the problem by asking how the Zeeman spin splitting caused by the magnetic field combines with the spin splitting caused by the BIA. An important advantage of the 5LM is that it includes the BIA mechanism of the spin splitting. In the following we will be concerned with symmetric quantum wells, so that the Bychkov-Rashba spin splitting, caused by the structure-inversion asymmetry, does not come into play.[10]

In studying orbital and spin electron energies in GaAs/$Ga_{1-x}Al_xAs$ single quantum wells other authors used an expansion of the conduction-band nonparabolic dispersion $\mathcal{E}(\mathbf{P})$, in powers of the generalized momentum $\mathbf{P}=\mathbf{p}+e\mathbf{A}$.[11,12] This was first developed by Ogg.[13] In the above method, the expansion coefficients for GaAs are taken from bulk magneto-optical data. The electric potential of the well is added at the end, so that this approach can be qualified as semiclassical. The band-edge values of m_0^* and g_0^* for the bulk $Ga_{1-x}Al_xAs$ are taken into account but the expansion coefficients for the dispersion $\mathcal{E}(k)$ are taken the same as for

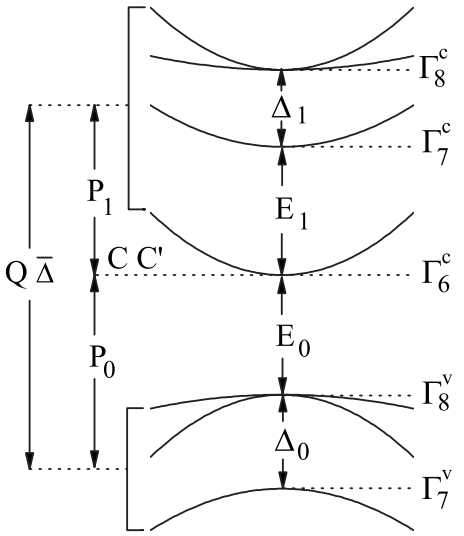

FIG. 1. Five-level model for the band structure of GaAs-type semiconductors. Energy gaps, spin-orbit energies, and interband matrix elements of momentum and of the spin-orbit interaction are indicated. Letters C and C′ mark symbolically far-band contributions to the effective mass and the spin g^* factor of conduction electrons, respectively.

GaAs. The final results obtained by this method are qualitatively similar to ours but quantitatively they are not the same (see Ref. 7). Our approach uses fundamental band parameters (energy gaps, spin-orbit energies, and momentum matrix elements), includes the heterostructure potential from the very beginning and is, in the final count, more exact. Last, but not least, the Ogg formalism is valid only for weakly nonparabolic energy bands since it is an expansion up to the $\mathbf{P}^4$ terms. On the other hand, our approach is valid also for narrow-gap systems because it takes *exactly* into account five interacting bands, see discussion in Ref. 7.

Our paper is organized as follows. In Sec. II the $\mathbf{P}\cdot\mathbf{p}$ theory using 5LM is briefly presented. In Sec. III A the 5LM is used to calculate the electron-spin g values for SLs. Section III B contains description of experimental effective masses in GaAs/$Ga_{1-x}Al_xAs$ SLs for both $\mathbf{B}_\parallel$ and $\mathbf{B}_\perp$ field configurations. In Sec. III C we study orbital properties of electrons in very short SLs in the $\mathbf{B}_\perp$ configuration and report on until now unobserved states. The paper is concluded by a summary.

II. THEORY

Our calculation of the spin and the cyclotron electron energies in GaAs/$Ga_{1-x}Al_xAs$ is based on the five-level $\mathbf{P}\cdot\mathbf{p}$ model. The 5LM includes explicitly the Γ_8^c, Γ_7^c, Γ_6^c, Γ_8^v, and Γ_7^v levels of the band structure at the center of the Brillouin zone, see Fig. 1. There exist three interband matrix elements of momentum: P_0, P_1, and Q, and three matrix elements of the spin-orbit interaction: Δ_0, Δ_1, and $\bar{\Delta}$ (see the definitions in Ref. 6). Within 5LM, there are 14 basis (Luttinger-Kohn) functions and the resulting eigenenergy problem consists of 14 coupled differential equations. We solve the equations by substitution. This is not possible exactly, so we use an iteration procedure with respect to the matrix elements Q (to the order of Q^2 terms). After considerable manipulation the effective Hamiltonian for the spin-up and spin-down electron states in the conduction band is obtained. In addition to the approach presented in Ref. 7 we include the off-diagonal free-electron term in the initial $\mathbf{P}\cdot\mathbf{p}$ 14×14 matrix. The general theoretical framework is the same for $\mathbf{B}$ parallel and transverse to the growth direction. We keep $\mathbf{B}\|\mathbf{z}$ in both cases and use the vector potential $\mathbf{A}=[-By,0,0]$. In the parallel case the SL potential $V(z)$ changes in the $\mathbf{z}$ direction, while in the transverse case the SL potential $V(y)$ changes in the $\mathbf{y}$ direction. The effective 2×2 Hamiltonian for electrons in the conduction Γ_6^c band is, for both field configurations,

$$\hat{H}=\begin{bmatrix}\hat{A}^+ & \hat{K}\\ \hat{K}^\dagger & \hat{A}^-\end{bmatrix}, \tag{1}$$

where

$$\hat{A}^+ = V(x_i)+\frac{1}{2}\sum_{i=1}^{3}P_i\frac{1}{m_I^*(\mathcal{E},x_i)}P_i+\frac{E_B}{2}g_I^*(\mathcal{E},x_i) + E_{P_0}E_B\frac{K_{11}}{2m_0}P_-P_+-\frac{E_Q}{12m_0^2}(E_{P_0}D_0+E_{P_1}D_1), \tag{2}$$

where

$$D_0=P_z(K_1P_-P_++K_2P_+P_-)P_z+2(K_5P_-P_+P_-P_++K_6P_+^2P_-^2 + K_7P_-^2P_+^2) \tag{3}$$

and

$$D_1=P_z(K_3P_-P_++K_4P_+P_-)P_z+2(K_8P_-P_+P_-P_++K_9P_+^2P_-^2 + K_{10}P_-^2P_+^2). \tag{4}$$

In the expression for $\hat{A}^-$ one should change the sign of g_I^* and K_{11} terms and exchange P_+ with P_-. The functions K_i, for $i=1,2,3,\ldots,10$, are defined in Ref. 7, $K_{11}=8/(9\tilde{E}_0\tilde{G}_0)$ and $E_B=\mu_B B$, where $\mu_B=e\hbar/2m_0$ is the Bohr magneton.

The effective mass m_I^* is

$$\frac{m_0}{m_I^*(\mathcal{E},x_i)}=1+C-\frac{1}{3}\left[E_{P_0}\left(\frac{2}{\tilde{E}_0}+\frac{1}{\tilde{G}_0}\right)+E_{P_1}\left(\frac{2}{\tilde{G}_1}+\frac{1}{\tilde{E}_1}\right) + \frac{4\bar{\Delta}\sqrt{E_{P_0}E_{P_1}}}{3}\left(\frac{1}{\tilde{E}_1\tilde{G}_0}-\frac{1}{\tilde{E}_0\tilde{G}_1}\right)\right] \tag{5}$$

and the g_I^* factor is

$$g_I^*(\mathcal{E},x_i)=2+2C'-2E_{P_0}C_f\frac{\partial}{\partial z}K_{11}\frac{\partial}{\partial z}+\frac{2}{3} \times\left[E_{P_0}\left(\frac{1}{\tilde{E}_0}-\frac{1}{\tilde{G}_0}\right)+E_{P_1}\left(\frac{1}{\tilde{G}_1}-\frac{1}{\tilde{E}_1}\right) - \frac{2\bar{\Delta}\sqrt{E_{P_0}E_{P_1}}}{3}\left(\frac{2}{\tilde{E}_1\tilde{G}_0}+\frac{1}{\tilde{E}_0\tilde{G}_1}\right)\right], \tag{6}$$

where

$$\tilde{E}_i = E_i - \mathcal{E} + V(x_i), \tag{7}$$

$$\tilde{G}_i = G_i - \mathcal{E} + V(x_i). \tag{8}$$

We use the notation $E_{P_0}=2\hbar^2P_0^2/m_0$, $E_{P_1}=2\hbar^2P_1^2/m_0$, and $E_Q=2\hbar^2Q^2/m_0$. The mass m_I^* and the factor g_I^* defined in Eqs. (5) and (6) do not represent final electron values in an SL but only the first iterative approximations to these quantities, see Ref. 7.

For GaAs quantum wells (QWs) we use $m^*/m_0=0.066$, $g^*=-0.44$ and, the energy band parameters: $E_0=-1.519$ eV, $E_1=2.969$ eV, $G_0=E_0+\Delta_0=-1.86$ eV, and $G_1=E_1+\Delta_1=3.14$ eV. For $Ga_{1-x}Al_xAs$ barriers we use: $m^*/m_0=0.066+0.0174x+0.145x^2$,[14] $g^*=-0.44+4.25x-3.9x^2$,[15] $V_B=0.8x$ eV, and $E_0=-(1.519+1.36x+0.22x^2)$ eV, $E_1=(2.969+0.971x)$ eV, $G_0=E_0+\Delta_0=-(1.86+1.229x+0.291x^2)$ eV, and $G_1=E_1+\Delta_1=(3.14+0.98x)$ eV, where x is the Al content (cf. Ref. 7). The interband matrix elements of momentum and of the spin-orbit interaction are taken to be independent of x: $E_{P_0}=27.865$ eV, $E_{P_1}=2.361$ eV, $E_Q=15.563$ eV, and $\bar{\Delta}=-0.061$ eV.

The interband matrix elements of momentum are defined as

$$P_0 = \frac{-i\hbar}{m_0\Omega}\langle S|p_x|X\rangle,$$

$$P_1 = \frac{-i\hbar}{m_0\Omega}\langle S|p_x|X'\rangle,$$

$$Q = \frac{-i\hbar}{m_0\Omega}\langle X|p_y|Z'\rangle = \frac{i\hbar}{m_0\Omega}\langle X'|p_y|Z\rangle \tag{9}$$

and the spin-orbit energies are

$$\Delta_0 = \frac{-3i\hbar}{4m_0^2c^2}\langle X|[\boldsymbol{\nabla}V_0,\mathbf{p}]_y|Z\rangle,$$

$$\Delta_1 = \frac{-3i\hbar}{4m_0^2c^2}\langle X'|[\boldsymbol{\nabla}V_0,\mathbf{p}]_y|Z'\rangle,$$

$$\bar{\Delta} = \frac{-3i\hbar}{4m_0^2c^2}\langle X|[\boldsymbol{\nabla}V_0,\mathbf{p}]_y|Z'\rangle. \tag{10}$$

The nondiagonal component in Eq. (1), related to the bulk inversion asymmetry, is a sum of two terms

$$\hat{K} = \hat{B}_1 + \hat{B}_2, \tag{11}$$

where

$$\hat{B}_1 = \frac{\sqrt{2}}{\hbar^3}\gamma(\mathcal{E},x_i)\left[P_+P_z^2 - \frac{1}{4}(P_-P_+^2 + P_+^2P_-)\right], \tag{12}$$

$$\hat{B}_2 = \frac{1}{\sqrt{2}\hbar^3}\gamma(\mathcal{E},x_i)P_-^3, \tag{13}$$

in which

$$\gamma(\mathcal{E},x_i) = \frac{4Q}{3}\left\{P_0P_1\left(\frac{1}{\tilde{G}_0\tilde{G}_1} - \frac{1}{\tilde{E}_0\tilde{E}_1}\right) - \frac{\bar{\Delta}}{3}\left[\frac{P_0^2}{\tilde{E}_0\tilde{G}_0}\left(\frac{2}{\tilde{E}_1}+\frac{1}{\tilde{G}_1}\right) - \frac{P_1^2}{\tilde{E}_1\tilde{G}_1}\left(\frac{2}{\tilde{G}_0}+\frac{1}{\tilde{E}_0}\right)\right]\right\}. \tag{14}$$

Since in both parallel and transverse configurations we keep $\mathbf{B}\|\mathbf{z}$, we have for $\hat{P}_\pm=(1/\sqrt{2})(P_x\pm iP_y)$ the same forms

$$P_\pm = \frac{\hbar}{\sqrt{2}}\left(k_x - \frac{eBy}{\hbar} \pm \frac{\partial}{\partial y}\right). \tag{15}$$

For the parallel case $\mathbf{B}_\parallel$, when $x_i=z$, the motion components along $\mathbf{z}$ and in the plane $\mathbf{x}$-$\mathbf{y}$ may be separated, the wave functions have the general form $\Psi=\exp(ik_xx)\Phi_n(y-y_0)\chi_l(z)$, where Φ_n are the harmonic oscillator functions, and the $\hat{P}_\pm$ operators raise and lower the $\exp(ik_xx)\Phi_n(y-y_0)$ functions. The main kinetic term in Eq. (2) takes then the form $p_z[1/2m_I^*(\mathcal{E},z)]p_z+[1/2m_I^*(\mathcal{E},z)](P_x^2+P_y^2)$. The corresponding calculations are presented in Ref. 7.

In the following we concentrate more on the transverse configuration $\mathbf{B}_\perp$ for which $x_i=y$. In this case the motion components along $\mathbf{z}$ and in the $\mathbf{x}$-$\mathbf{y}$ plane are not separable, the wave functions have the general form $\Psi=\exp(ik_xx+ik_zz)\chi_l(y-y_0)$, and the operators $P_\pm$ of Eq. (15) do not have raising and lowering properties, see Ref. 7.

Acting on the above wave functions the operator $\hat{p}_x$ gives $\hbar k_x$ and $\hat{p}_z$ gives $\hbar k_z$. Since we are interested in the undoped SLs we assume that the Fermi energy coincides with the ground electric subband, so that

$$k_z = 0. \tag{16}$$

In this case the corresponding terms in the effective Hamiltonian are

$$\hat{A}^\pm = V(y) - C_f\frac{\partial}{\partial y'}\frac{m_0}{m_I^*(\mathcal{E},y')}\frac{\partial}{\partial y'} + \frac{C_fm_0}{m_I^*(\mathcal{E},y')}\frac{y'^2}{L^4} \pm \frac{E_B}{2}g_I^*(\mathcal{E},y') \pm E_{P_0}E_BC_f\left(\frac{y'^2}{L^4}K_{11} - \frac{\partial}{\partial y'}K_{11}\frac{\partial}{\partial y'}\right) \pm \frac{E_QE_BC_f}{3}\left(\frac{\partial}{\partial y'}F_1\frac{\partial}{\partial y'} - \frac{2y'^2}{L^4}F_2\right), \tag{17}$$

where $y'=y-k_xL^2$, in which the magnetic radius is $1/L^2=eB/\hbar$ and $C_f=\hbar^2/(2m_0)$. Further

$$F_1 = E_{P_0}(K_5 - 2K_6 + 2K_7) + E_{P_1}(K_8 - 2K_9 + 2K_{10}), \tag{18}$$

$$F_2 = E_{P_0}(K_5 - K_6 + K_7) + E_{P_1}(K_8 - K_9 + K_{10}), \tag{19}$$

and

$$\hat{K} = -\gamma(\mathcal{E}, y')\left[\frac{y'}{L^4}\left(1 + y'\frac{\partial}{\partial y'}\right) + \frac{1}{L^2}\left(\frac{\partial}{\partial y'} + y'\frac{\partial^2}{\partial y'^2}\right)\right]. \tag{20}$$

As to the periodic potential of an SL, we consider the Kronig-Penney rectangular GaAs wells of the width a separated by rectangular $Ga_{1-x}Al_xAs$ barriers of the width b. Barriers terminating the SL on both ends are assumed to be made of the same barrier material $Ga_{1-x}Al_xAs$. We use the simple boundary conditions at the interfaces

$$\chi_l|_+ = \chi_l|_-, \tag{21}$$

$$\left(\frac{1}{m_+^*}\frac{\partial \chi_l(x_i)}{\partial x_i}\right)_+ = \left(\frac{1}{m_-^*}\frac{\partial \chi_l(x_i)}{\partial x_i}\right)_-. \tag{22}$$

The more complete boundary conditions include the nondiagonal spin-dependent terms due to BIA, as seen in Eqs. (1) and (11). If BIA mechanism is treated by perturbation theory, the zero-order solutions (and the corresponding boundary conditions) do not contain the off-diagonal BIA terms and the latter is included in the form of the matrix element of perturbation. We checked that this procedure gives a very good approximation to the final energies, as compared to the exact procedure including BIA also in the boundary conditions. The above simplified procedure gives excellent results for the spin g values in GaAs/GaAlAs quantum wells, see Ref. 7. Finally, as indicated below, for the transverse-field configuration the BIA mechanism vanishes and also the exact boundary conditions do not contain the off-diagonal BIA terms.

The eigenenergy is found requiring that the wave function goes to zero at sufficiently far distances on both sides. It is important that we treat the whole SL as a potential well, so that the electron wave functions are standing waves, not the running Bloch waves. This problem is discussed in some detail in our recent work.[16]

The above theory describes both the nonparabolicity and the nonsphericity of conduction band in III-V compounds. The nonparabolicity is expressed by energy and potential dependence of $m_l^*(\mathcal{E}, x_i)$ and $g_l^*(\mathcal{E}, x_i)$ in Eqs. (5) and (6). The nonsphericity is related to the matrix element Q and is expressed by the terms proportional to E_Q. The contributions related to the nondiagonal free-electron terms in the initial $\mathbf{P}\cdot\mathbf{p}$ matrix are proportional to K_{11}. As mentioned above, the nondiagonal term $\hat{K}$ in Hamiltonian (1), related to the bulk-inversion asymmetry of III-V compounds, is described in the final form by Eq. (20). The simplest way to solve the 2×2 problem posed by Hamiltonian (1) is to find eigenfunctions and eigenvalues of the diagonal terms and to calculate the matrix elements of the nondiagonal terms. Since we treat rectangular (i.e., symmetric) SLs, the wave functions of the miniband for both spins are described by an even or an odd function $\chi_l(y)$. On the other hand, it can be seen from Eq. (20) that the off-diagonal terms $\hat{K}$ are odd functions of y. As a consequence, the matrix element of the off-diagonal terms vanishes and we are left with the eigenvalues of the diagonal terms. Strictly speaking, the BIA mechanism does not come into play for the $\mathbf{B}_\perp$ configuration if the center of magnetic potential is chosen in the middle of the structure. When the BIA mechanism for the spin splitting is not active or is neglected, the spin g factor in III-V compounds varies as a function of increasing electron energy from the band-edge value g_0^* to the free-electron value +2.[17] However, the BIA spin splitting does not obey this rule.

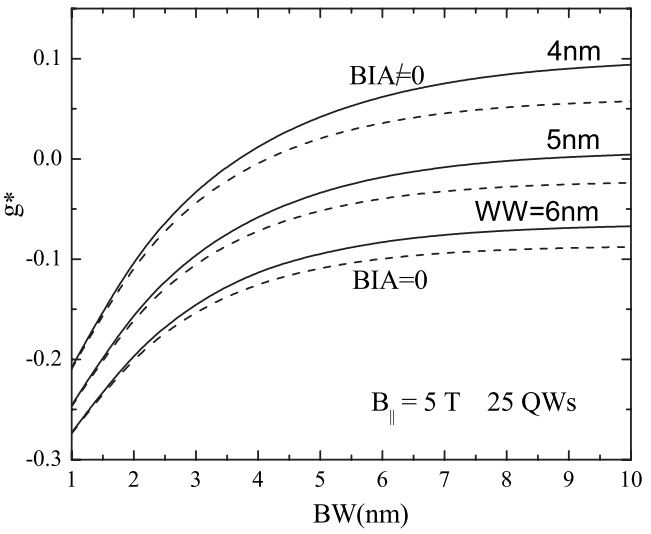

FIG. 2. Calculated spin g factor of electrons in $GaAs/Ga_{0.7}Al_{0.3}As$ superlattices in longitudinal-field configuration for three well widths versus barrier widths. Dashed lines—neglecting BIA mechanism, solid lines—including BIA mechanism.

III. RESULTS

Below we use our theory to calculate electron-spin g values in $GaAs/Ga_{1-x}Al_xAs$ SLs and to describe some existing experimental data on the effective cyclotron masses for both $\mathbf{B}_\parallel$ and $\mathbf{B}_\perp$ configurations. In addition, we predict and

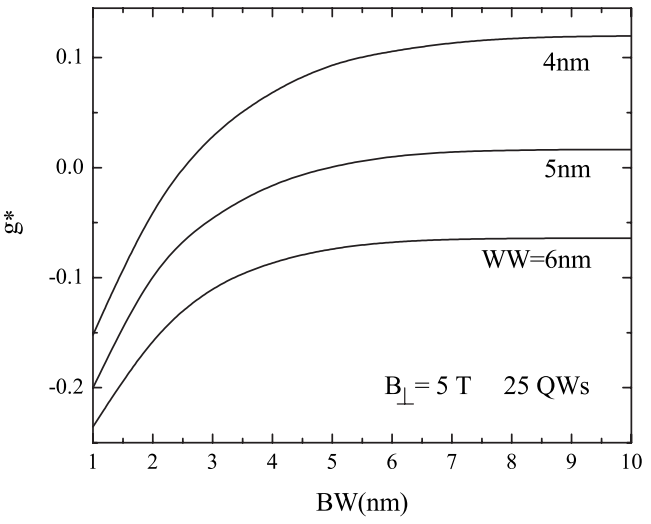

FIG. 3. The same as in Fig. 2, but for the transverse-field configuration. The BIA mechanism of spin splitting is not active for $\mathbf{B}_\perp$.

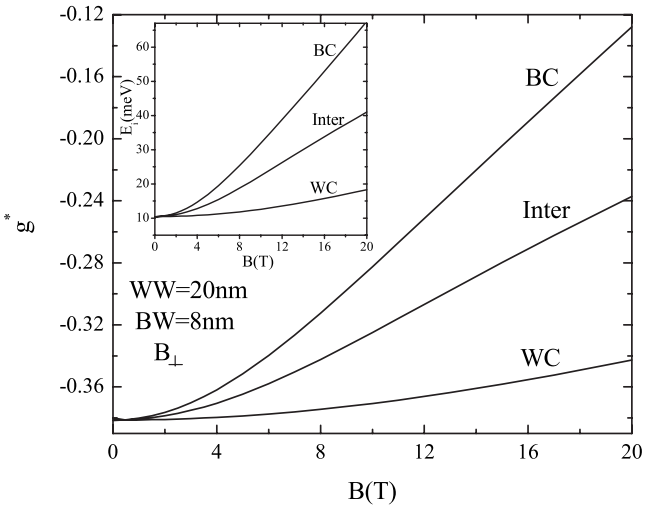

FIG. 4. Calculated spin g factors of electrons in GaAs/$Ga_{0.7}Al_{0.3}As$ superlattices in the transverse-field configuration versus field intensity $\mathbf{B}_\perp$ for three centers of magnetic oscillations $y_0=k_xL^2$: WC—well center, Inter—interface, and BC—barrier center. The inset shows corresponding electron energies.

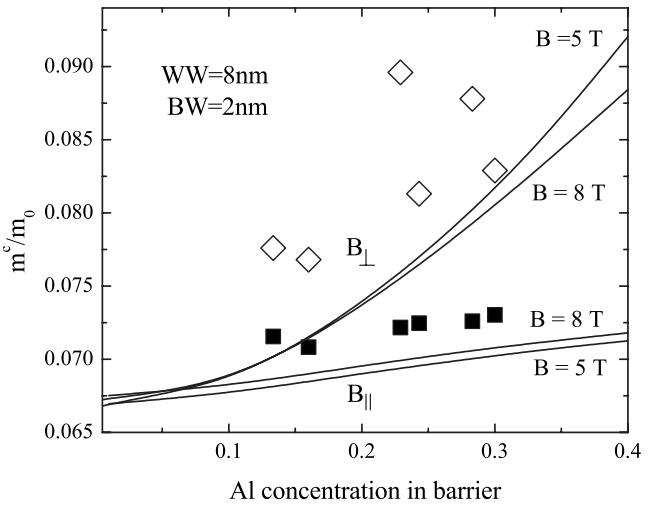

FIG. 5. Measured and calculated cyclotron masses in GaAs/$Ga_{1-x}Al_xAs$ superlattices for longitudinal- and transverse-field configurations $\mathbf{B}_\parallel$ and $\mathbf{B}_\perp$ versus Al content x in the barriers. Solid lines are theoretical. Solid squares—$m^c_\parallel$ measured by Duffield *et al.* (Ref. 19) for $\mathbf{B}_\parallel$, empty squares—$m^c_\perp$ retrieved from Ref. 19 using measured values of $m^c_\parallel$, and quoted values of m_{tr} with the use of relation $(m^c_\perp)^2=m^c_\parallel m_{tr}$.

describe unexpected orbital energies and states in short SLs in the presence of a transverse magnetic field $\mathbf{B}_\perp$.

A. Spin g values

In Fig. 2 we show the calculated electron g values in GaAs/$Ga_{1-x}Al_xAs$ SLs (parallel configuration $\mathbf{B}_\parallel$) for given well widths (WWs) as functions of barrier widths (BWs). For a fixed BW, the g value increases as the well becomes narrower. This is a direct result of nonparabolicity. When the wells are narrow, the electron energy increases and the g factor increases from the bulk value −0.44 tending to the value +2. For a fixed WW, the g factor increases with the growing BW because a bigger part of the electron wave function is in the $Ga_{1-x}Al_xAs$ region. The bulk-inversion asymmetry is seen to increase the g value. Its role increases as the wells become narrower because the value of k_z "frozen" in the narrower wave function increases. (The latter should not be confused with the k'_z arising due to the periodicity of an SL.) For large barrier widths the properties of electrons in SLs approach those in a single QW. Indeed, the g values shown in Fig. 2 in the above limit are similar to the values calculated in Ref. 7.

Figure 3 shows the calculated spin g values for the transverse configuration $\mathbf{B}_\perp$. The qualitative and the quantitative behaviors of g is similar for the two configurations. The main difference with the parallel configuration $\mathbf{B}_\parallel$ is that, as mentioned in the previous section, the BIA mechanism is not active for $\mathbf{B}_\perp$.

Finally, we investigate a dependence of the spin g factor on a position of the center of magnetic oscillations $y_0=k_xL^2$ in the transverse configuration $\mathbf{B}_\perp$. In Fig. 4 we show the calculations of $g^*(\mathbf{B}_\perp)$ for three positions of y_0: (1) at the center of a well, (2) at an interface, and (3) at the center of a barrier. It is seen that the spin factor is clearly different for the three situations. The differences are due to band's nonparabolicity. It can be seen from the inset that the electron energies in the three situations are considerably different. Since at low temperatures the electrons will occupy the lowest possible energies, they will be located near the well center, so that in practice the g factor will be described by the lowest line in Fig. 4. Thus, although one can speak, *in principle*, of a breakdown of the $\mathbf{P}\cdot\mathbf{p}$ description also for the spin properties (in analogy to the effective mass, see Ref. 18), *in practice* the effects related to such breakdown should be small. This result is somewhat paradoxical: it is because of the large energy differences for various y_0 that the electrons contributing to the spin properties will come from well-defined regions of y_0 and the differences in g values will not come into play. It should be mentioned that the electron-energy differences for various y_0 calculated in Ref. 18 are considerably smaller than those shown in the inset of Fig. 4. As a consequence, also the differences of the spin g values for various y_0 are very small. The reason is that the authors of Ref. 18 considered much narrower barriers in their SL.

B. Effective masses

Now we want to discuss some aspects of the orbital behavior of electrons in SLs and, in particular, to describe existing cyclotron resonance (CR) experimental data. To avoid confusion, we clearly define three effective masses of interest. And so, $m^c_\parallel$ is the mass *measured* in the cyclotron resonance for $\mathbf{B}_\parallel$ while $m^c_\perp$ is the mass measured for $\mathbf{B}_\perp$. Finally, the so-called transport mass m_{tr} is related to the energy dispersion of an SL miniband $\mathcal{E}(k'_z)$. This mass is given by $1/m_{tr}=(1/\hbar^2k'_z)\partial\mathcal{E}(k'_z)/\partial k'_z$. It is usually assumed that the three masses are related by the formula $m_{tr}=(m^c_\perp)^2/m^c_\parallel$, see the discussion below.

In Fig. 5 we show the data of Duffield *et al.*[19] on $m^c_\parallel$, as

measured by the CR in GaAs/$Ga_{1-x}Al_xAs$ SLs for different Al content in barriers. There is a slight increase in the mass due to band's nonparabolicity related to the fact that, as the barrier height increases with the Al content, the electron energy becomes larger. Also, a higher Al content makes the mass in $Ga_{1-x}Al_xAs$ higher, so the average mass increases. We added the point for $x=0.3$ (not shown in Fig. 3 of Ref. 19) which we determined from the data given in Fig. 2 of Ref. 19. Our theoretical curves reproduce well the data, apart from the fact that, using the accepted band-edge mass value $m_0^*=0.066m_0$, the theory predicts somewhat lower masses than the observed values.

As to the transverse configuration $\mathbf{B}_\perp$, the experimental values of $m_\perp^c$, shown in Fig. 5, have been retrieved employing the formula $m_{tr}=(m_\perp^c)^2/m_\parallel^c$ using the measured values of $m_\parallel^c$ and *given* values of m_{tr}, as quoted in Ref. 19 (see also Ref. 12). Again, we added the values of $m_\perp^c$ and $m_\parallel^c$ for Al content $x=0.3$ determined from the data given in Ref. 19. Our theory gives a reasonable description of the experimental data. One could get a better fit to the measured values taking a higher band-edge mass, but there is no reason to do that. The fact that the experimental data for both $m_\parallel^c$ and $m_\perp^c$ run higher than the theory predicts can be attributed either to a small admixture of Al in the GaAs wells (which is not very probable) or to a nonvanishing free-electron density in the investigated SLs. In fact, Duffield *et al.*[18] observed directly a nonvanishing free-electron density in similar structures.

Finally, we check the validity of the relation $m_{tr}=(m_\perp^c)^2/m_\parallel^c$ for our SLs. Namely, we can *compute* separately $m_\parallel^c$ and $m_\perp^c$ for low-lying Landau levels in both field configurations and *calculate* independently the transport mass $1/m_{tr}=(1/\hbar^2k_z')\,\partial\mathcal{E}(k_z')/\partial k_z'$, computing prior to that the $\mathcal{E}(k_z')$ relation for the electric miniband at $B=0$. In Fig. 6 we show the results of such calculations for varying Al content in the barriers. The solid line shows calculated m_{tr} while the dashed line indicates the calculated value of $(m_\perp^c)^2/m_\parallel^c$. It can be seen that, while the two quantities coincide quite well for an SL with high barriers (high Al content), the coincidence becomes poorer for an SL with low barriers. It should be mentioned that our calculations are carried out assuming the confining barriers at both ends of an SL to be of the same heights as the inside barriers (i.e., for the same $Ga_{1-x}Al_xAs$ material). On the other hand, "experimental" $m_\perp^c$ values retrieved from Ref. 19 and shown in Fig. 5 do not depend on the validity of the above relation, since both Duffield *et al.*[19] and us used the same formula.

C. New orbital states

Finally, we consider very short SLs or, more precisely, a few periodic quantum wells placed in a transverse external field $\mathbf{B}_\perp$. This configuration was considered before by Zawadzki,[20] Maan and others,[21–23] and Duffield *et al.*[18,19] and it was shown both theoretically and experimentally that the orbital electron energies in this situation depend on a position of the center of magnetic oscillations $y_0=k_xL^2$. Three types of magnetic orbits were identified depending on whether an electron is located in the center of a QW, near its wall (interface) or at the barrier. The dependence of electron

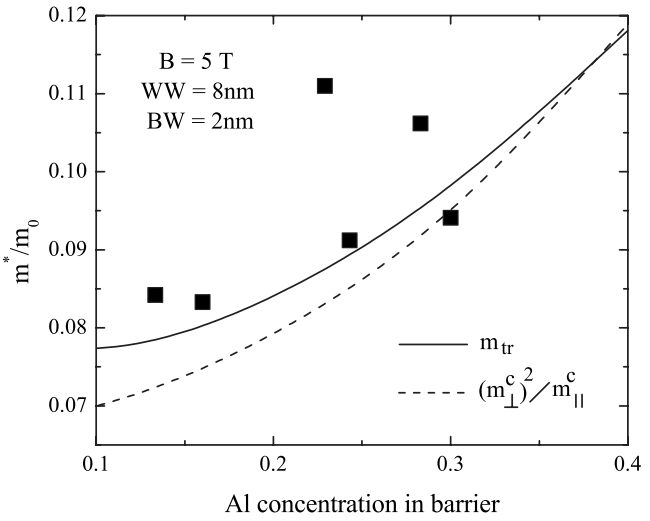

FIG. 6. "Transport" mass calculated directly for GaAs/$Ga_{1-x}Al_xAs$ superlattices: $1/m_{tr}=(1/\hbar^2k_z')\,\partial\mathcal{E}(k_z')/\partial k_z'$, compared to calculated values of $(m_\perp^c)^2/m_\parallel^c$ versus Al content x in the barriers. Full squares indicate experimental values of $(m_\perp^c)^2/m_\parallel^c$ as determined in Ref. 19.

energies on the spacial position of the center y_0 means that the usual description of the cyclotron frequency $\omega_c=eB/m^*$ by means of the effective mass breaks down. One can interpret this phenomenon as another manifestation of the property mentioned above that, in the transverse-field configuration $\mathbf{B}_\perp$, one may not separate the magnetic component of the motion from its electric component. This leads to various "anomalies" and "breakdowns." In our opinion, one should carefully distinguish between the effective-mass approximation, which is used in the initial Schrodinger equation involving the periodic potential of a heterostructure and an external magnetic field, and the effective mass describing the final energies. It is, in general, not surprising that in a spacially inhomogeneous system the electron energy depends on the center of magnetic oscillations.

We begin our considerations by a single rectangular QW (finite or "infinitely" high) of the width a placed in a transverse magnetic field $\mathbf{B}_\perp$. It was shown in Ref. 20 that, as $\mathbf{B}_\perp$ increases from zero to high values, the electric quantization goes over to the magnetic quantization (Landau levels). The important parameter in the problem is a/L, where $L=(\hbar/eB)^{1/2}$ is the magnetic radius. When $a/L\ll 1$, the motion (and quantization) is of the electric type; for $a/L\gg 1$ the motion (and quantization) is of the magnetic type.

Next, we consider a structure of two rectangular quantum wells made of GaAs and $Ga_{1-x}Al_xAs$. As before, the well width is $a=20$ nm, the barrier width is $b=8$ nm, and the barrier height is 240 meV. The center of magnetic oscillations $y_0=k_xL^2$ is chosen at the center of the right well. To simplify the problem we neglect the spin energies, band's nonparabolicity, and mass difference between GaAs and $Ga_{1-x}Al_xAs$, taking $m_0^*=0.066m_0$. Thus, we solve the simple Schrodinger equation

$$\left[\frac{-\hbar^2\partial^2}{2m_0^*\,\partial y^2}+V(y)+\frac{m_0^*\omega_c^2}{2}(y-y_0)^2\right]\Psi=\mathcal{E}\Psi, \qquad (23)$$

using the standard boundary conditions. Here $\omega_c=eB/m_0^*$.

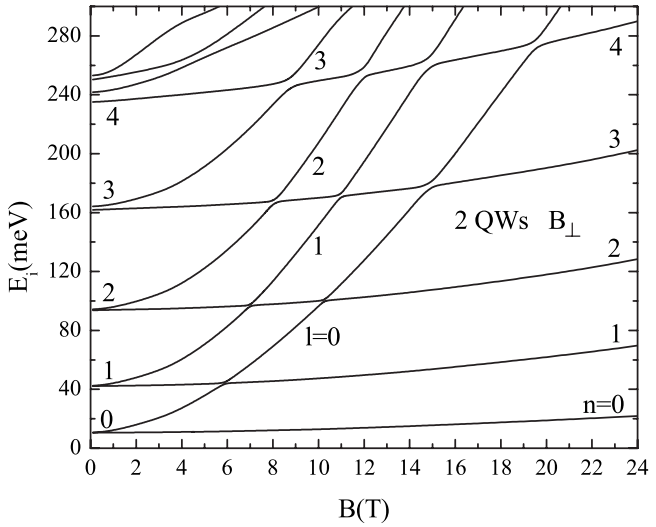

FIG. 7. Calculated energies of orbital electron states in $GaAs/Ga_{0.7}Al_{0.3}As$ two QWs versus transverse magnetic field intensity $\mathbf{B}_\perp$. At $\mathbf{B}_\perp=0$ the levels are quantized into electric doublets, at high fields one deals with the Landau levels. At intermediate fields there appears a family of states whose energies have strong, almost quadratic $\mathbf{B}_\perp$ dependences, see text.

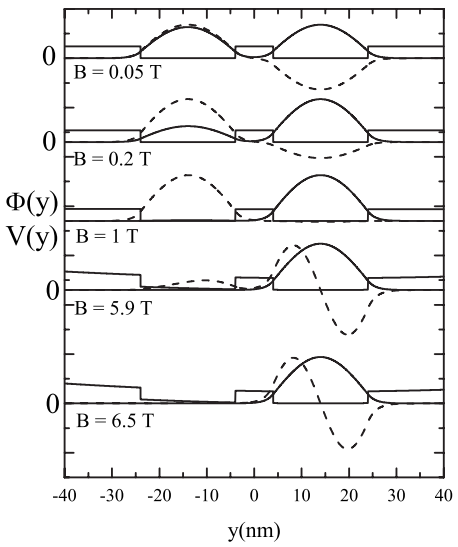

FIG. 8. Evolution of the wave functions describing two lowest levels in an SL of two QWs for increasing transverse magnetic field $\mathbf{B}_\perp$. The center of magnetic oscillations is chosen in the middle of the right QW. As $\mathbf{B}_\perp$ grows, the function $0l$ (solid line) moves into the right QW while the function $0u$ (dashed line) moves first to the left QW and then to the right QW, see text. Both QW profiles and the magnetic parabola are also indicated.

In Fig. 7 we show the calculated electron energies plotted versus increasing magnetic field $\mathbf{B}_\perp$. For vanishing $\mathbf{B}_\perp$ we obtain, as expected, electric quantization similar to that in a single QW. The difference is that, instead of single levels (without spin), the levels occur in pairs. For high $\mathbf{B}_\perp$ the situation is again similar to a single well, i.e., one has the Landau levels. However, in the intermediate range of $\mathbf{B}_\perp$ we deal with an unexpected picture. Higher levels of each "electric" pair move upward with $\mathbf{B}_\perp$ much faster than the lower levels, they undergo anticrossings with the upper slowly moving levels and form, in an overall behavior, separate set of energy levels moving upwards with $\mathbf{B}_\perp$ much faster than the regular Landau levels. They have roughly $\mathcal{E}(\mathbf{B}_\perp)\sim\mathbf{B}_\perp^{1.94}$ dependence. Clearly, electrons in the center of the left well will have the same energies since their location is exactly symmetric to the one considered above. Thus, we believe that the situation shown in Fig. 7 is quite realistic.

A somewhat similar behavior of energy levels is observed for a donor atom in a magnetic field $\mathbf{B}$. At vanishing B one deals with hydrogenlike electric levels. For low B these levels undergo diamagnetic shifts, at high B the Landau levels are formed, each having a ladder of donor levels attached to it.[24]

In order to get some insight into the level behavior indicated in Fig. 7, we show evolutions of the wave functions for the lowest pair of levels, see Fig. 8. At $\mathbf{B}_\perp\approx 0$, the lower level $0l$ is described by a symmetric function and the upper one $0u$ by an antisymmetric function. At a low field $\mathbf{B}_\perp=0.2$ T the $0l$ function begins to disappear in the right QW and the $0u$ function begins to disappear in the left QW. At $\mathbf{B}_\perp\approx 1$ T this process is practically finished; the $0l$ function is completely in the right QW and it stays there at all higher $\mathbf{B}_\perp$, so the $0l$ energy behaves like in a one-well system and it begins to represent the $n=0$ Landau level. The $0u$ function stays in the left QW until a certain critical field $\mathbf{B}_\perp^{cr}$. It is in this range of $\mathbf{B}_\perp$ that the $0u$ energy changes quickly with $\mathbf{B}_\perp$ because the $0u$ function is at the shoulder of the magnetic parabola. At the critical field, which for our QWs is about 5.5 T, the $0l$ function begins to "escape" from the left QW to the right one. Once this process is accomplished at $\mathbf{B}_\perp=6.5$ T, the $0l$ state behaves at higher $\mathbf{B}_\perp$ like in a one-well system and it begins to represent the $n=1$ Landau level. Clearly, the above considerations do not really "explain" the appearance of the "quadratic" levels moving quickly upwards with $\mathbf{B}_\perp$. In particular, it is not intuitively clear why the antisymmetric

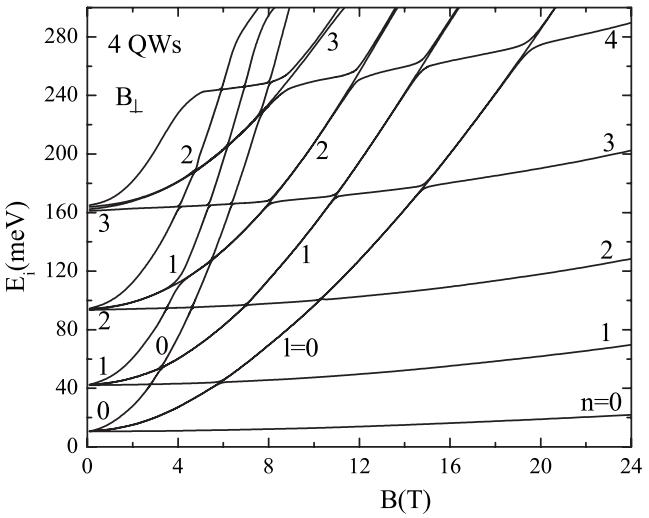

FIG. 9. The same as in Fig. 7 but for an SL of four QWs. At $\mathbf{B}_\perp=0$ the levels are quantized into minibands of four levels, at high fields one deals with the Landau levels. At intermediate fields there appear *two families* of states whose energies have strong quadraticlike $\mathbf{B}_\perp$ dependences.

function $0u$ moves first to the left QW at low $\mathbf{B}_\perp$. It is due to this effect that the level $0u$ depends strongly on $\mathbf{B}_\perp$.

We performed similar calculations for SLs having more QWs. The results for an SL of four QWs are shown in Fig. 9. The center of magnetic potential is chosen in the middle of the second QW from the rhs. The general scheme of levels is similar to that shown in Fig. 7, but there also appear significant differences. Of the four levels in each miniband at $\mathbf{B}_\perp=0$ the lowest level behaves "normally" and goes at higher fields to the $n=0$ Landau level. Two higher levels have very similar behavior as functions of $\mathbf{B}_\perp$ and they give rise to the $l=0$ quadratic level. The new feature is that the fourth, highest level has an even stronger dependence on $\mathbf{B}_\perp$ and gives rise to another family of levels. The second new feature seen in Fig. 9 is that certain levels go through the anticrossing regions without any deflection. Otherwise the energies shown in Figs. 7 and 9 are similar and the main new result remains the same: there appear states characterized by roughly quadratic dependences of their energies on the transverse magnetic field $\mathbf{B}_\perp$. This conclusion is valid also for SLs having many QWs.

The above states should be observable either in interband magneto-optical transitions or in CR-like intraband transitions. Belle *et al.*[21,22] measured magnetophotoluminescence in GaAs/GaAlAs superlattices for both $\mathbf{B}_\parallel$ and $\mathbf{B}_\perp$ field configurations but their experimental field of $\mathbf{B}=19$ T was too high to observe the states, cf. Fig. 9. A calculation of the matrix elements for optical transitions between states of the type shown in Fig. 8 offers some intricacies which we leave to a future publication. To conclude, we emphasize again that the results presented in Figs. 7–9 are calculated for a specific value of the center of magnetic oscillations located in the middle of the right (or left) quantum well. These points are the most probable (but not the only possible) electron locations at low temperatures.

IV. SUMMARY

We considered theoretically electrons in $GaAs/Ga_{1-x}Al_xAs$ superlattices and described their spin and orbital properties in the presence of an external longitudinal and transverse magnetic field. The spin g values are computed as functions of $Ga_{1-x}Al_xAs$ barrier widths for different GaAs well widths in both field configurations. Available measurements of cyclotron effective masses are described and a reasonable agreement between theory and experiment is reached. Investigating short superlattices in a transverse magnetic field $\mathbf{B}_\perp$ we found, in addition to the standard electric and Landau states, unexpected orbital states having a strong quadraticlike energy dependence $\mathcal{E}(\mathbf{B}_\perp)$. The origin of the states is investigated.

*pfeff@ifpan.edu.pl

[1] L. Esaki and R. Tsu, IBM J. Res. Dev. **14**, 61 (1970).
[2] G. Bastard, Phys. Rev. B **24**, 5693 (1981); **25**, 7584 (1982).
[3] D. L. Smith and C. Mailhiot, Phys. Rev. B **33**, 8345 (1986).
[4] G. Y. Wu, T. C. McGill, C. Mailhiot, and D. L. Smith, Phys. Rev. B **39**, 6060 (1989).
[5] N. F. Johnson, H. Ehrenreich, P. M. Hui, and P. M. Young, Phys. Rev. B **41**, 3655 (1990).
[6] P. Pfeffer and W. Zawadzki, Phys. Rev. B **41**, 1561 (1990); **53**, 12813 (1996).
[7] P. Pfeffer and W. Zawadzki, Phys. Rev. B **74**, 115309 (2006); **74**, 233303 (2006).
[8] P. von Allmen, Phys. Rev. B **46**, 15382 (1992).
[9] G. Dresselhaus, Phys. Rev. **100**, 580 (1955).
[10] Y. A. Bychkov and E. I. Rashba, J. Phys. C **17**, 6039 (1984).
[11] M. de Dios-Leyva, E. Reyes-Gomez, C. A. Perdomo-Leiva, and L. E. Oliveira, Phys. Rev. B **73**, 085316 (2006).
[12] A. Bruno-Alfonso, L. Diago-Cisneros, and M. de Dios-Leyva, J. Appl. Phys. **77**, 2837 (1995).
[13] N. R. Ogg, Proc. Phys. Soc. **89**, 431 (1966).
[14] B. El Jani, P. Gibart, J. C. Portal, and R. L. Aulombard, J. Appl. Phys. **58**, 3481 (1985).
[15] C. Weisbuch and C. Hermann, Phys. Rev. B **15**, 816 (1977).
[16] P. Pfeffer and W. Zawadzki, Semicond. Sci. Technol. **24**, 105002 (2009).
[17] W. Zawadzki, Phys. Lett. **4**, 190 (1963).
[18] T. Duffield, R. Bhat, M. Koza, D. M. Hwang, F. DeRosa, P. Grabbe, and S. J. Allen, Jr., Solid State Commun. **65**, 1483 (1988).
[19] T. Duffield, R. Bhat, M. Koza, F. DeRosa, D. M. Hwang, P. Grabbe, and S. J. Allen, Jr., Phys. Rev. Lett. **56**, 2724 (1986).
[20] W. Zawadzki, Semicond. Sci. Technol. **2**, 550 (1987).
[21] G. Belle, J. K. Maan, and G. Weimann, Surf. Sci. **170**, 611 (1986).
[22] J. K. Maan, Festkoerperprobleme **27**, 137 (1987).
[23] J. K. Maan, Surf. Sci. **196**, 518 (1988).
[24] W. Zawadzki, in *Landau Level Spectroscopy*, edited by G. Landwehr and E. T. Rashba (North-Holland, Amsterdam, 1991), p. 1305.